Eur Biophys J (2009) 38:749–756
DOI 10.1007/s00249-009-0486-1

ORIGINAL PAPER

Brownian dynamics simulations reveal regulatory properties of higher-order chromatin structures

Jens Odenheimer · Dieter W. Heermann · Gregor Kreth

Received: 1 February 2009 / Revised: 6 May 2009 / Accepted: 13 May 2009 / Published online: 18 June 2009

Abstract A present model of the higher-order chromosome organization suggests the organization of chromosome built up by loops. Here we focus on a single rosette-like part of the fiber and analyse the diffusion behaviour of small particles (corresponding to single proteins/protein complexes) and the accessibility of such particles in relation to the dynamic rosette structure. Surprisingly, although the diffusion pattern of the diffusing particles revealed free diffusion, an area of about 6–12 kbp in the innermost part of these domains becomes visible which is inaccessible even for small particles (corresponding to single proteins/protein complexes). A localisation of a promotor sequence in this area might silence the respective gene by the physical inaccessibility of this area for transcription factors. We conclude that the compartmentalisation of chromatin in domains of a specific dynamical three-dimensional (3D) structure might be of high functional importance.

Keywords Intranuclear diffusion · Gene silencing · Brownian dynamics · Nuclear architecture · Computer modelling

This article has been submitted as a contribution to the festschrift entitled "Uncovering cellular sub-structures by light microscopy" in honour of Professor Cremer's 65th birthday.

J. Odenheimer · D. W. Heermann
Institute for Theoretical Physics, Heidelberg University, Philosophenweg 19, 69120 Heidelberg, Germany

G. Kreth (✉)
Kirchhoff Institute for Physics, Heidelberg University, INF 227, 69120 Heidelberg, Germany
e-mail: gkreth@kip.uni-heidelberg.de

Introduction

The dynamic regulation of chromatin accessibility for transcription during interphase is still a poorly understood topic in cell biology. In the past decade accumulating evidence has supported the view that the higher-order organisation of chromatin domains itself provides another level of epigenetic gene regulation, a view that is underpinned by the presented computer modelling approach. Presently, chromatin is typically classified into two distinct conformations: relatively uncondensed euchromatin and much denser chromatin regions referred to as heterochromatin. Heterochromatin is transcriptionally less active than euchromatin. The facultative part of heterochromatin, however, can transit to a more open, transcriptionally active conformation, which is characterised by its higher accessibility to various protein complexes. A number of studies have concluded that such a transition to a more open state is triggered by histone acetylation (e.g. Roh et al. 2005; Strahl and Allis 2000).

It was frequently postulated that an induction of a more open chromatin state in response to histone acetylation increases the accessibility of transcription complexes to genomic DNA and that this regulates gene expression. In a recent study, Gorisch et al. (2005) analysed chromatin accessibility in dependence on histone acetylation by visualising fluorescein-labelled dextrans of different sizes within the nuclear volume (Gorisch et al. 2005). These experiments clearly support a major influence of histone acetylation in the dynamic regulation of chromatin accessibility. Another important and possibly relevant finding for transcription processes is the observation that chromatin forms loops to bring distant genes together so that they can bind to local concentrations of relevant proteins of polymerases in "factories" or hubs. Bon et al. (2006)

performed Monte Carlo calculations of a semi-flexible (self-avoiding) tube attached to a sphere to find out how loop thickness, rigidity and contour length influence the probability of where particular segments of the loop are located in relation to binding sites on the sphere (Bon et al. 2006). From these calculations they proposed "cold" (genetically inactive) zones in the outer part of the loop and "hot" (genetically) active zones which are located closer to the base points of the loops. The importance of physical interactions between ties to form genomic loops and higher-order structures such as rosettes for (e.g. transcription) factory formation was reviewed also by Marenduzzo et al. (2007).

To explain recent experimental results showing that chromatin fiber at large genomic distances, >1–2 Mb, exhibits a leveling-off of the mean-square distance between two DNA sites, we recently proposed a Gaussian random loop polymer model (Bohn et al. 2007). According to this model, a given number of sites of distant beads, randomly selected along the chain, are bound by a harmonic potential. An evaluation of the mean distance between sites and the size of loops showed that the presence of random loops on all length scales explains the leveling-off of the mean-square distance. These findings are also close to the theoretical predictions of a recently published model of Nicodemi and Prisco (2009). In this model cross-interactions of DNA sites are mediated by the binding of molecular factors and by the formation of bridges. These model representations of the formation of loops in a random manner on different scales might be seen as a future development of the multi-loop subcompartment model (MLS) of Münkel and Langowski (1998) and the model of Ostashevsky (1998). Both models assumed the existence of predefined 1-Mbp-sized rosette-like structures with given loop size. Such rosettes were experimentally identified by the foci structure building up the chromosome territories (for an overview see Cremer and Cremer 2001).

Herein we take modelled rosette-like structures which are formed dynamically by a number of attractive sites distributed along the linear chromatin fiber (see Odenheimer et al. 2005) to study the motion of differently sized tracer particles in relation to the modelled chromatin structure by Brownian dynamics simulations.

Results

To relate diffusion of small particles in the neighbourhood of large chromatin domains, the diffusive properties of four differently sized particles are simulated. To allow a comparison with "real" protein complexes we adapt the mass and the dimension of the particles from the following substances: streptavidin (as an example for a typical small protein), green fluorescent protein proliferating cell nuclear antigen (GFP PCNA) trimer, RNA polymerase II and ribosomes (as an example of a large multi-protein complex). The masses and dimensions as well as the force fields and their respective cutoffs are given in Tables 1 and 2. For the modelling of the rosette structure, a similar mapping is used as that used by Odenheimer et al. (2005). To obtain the model of a rosette, which present the target for the Brownian dynamics simulation runs, a number of attractive sites are distributed along the linear chromatin fiber, which results in the formation of loop structures. These attractive sites can be distributed either in a random manner or at predefined distances. To investigate the diffusion behaviour under well-defined conditions, for the present simulations the attractive sites are distributed at predefined distances, which results in equal loop sizes of 120 kbp and an overall rosette size of 1.2 Mbp. The attractive interaction between these sites is realised by Lennard–Jones force fields (see section "Simulation techniques"). To obtain different intra-rosette spacings, i.e., different distances of the attractive sites, four different values of the parameter σ, ranging from 2.5 to 27.3 nm, for the Lennard–Jones interaction are investigated.

Table 1 Mass and dimensions of the simulated substances: 1 Da = 1 u (in SI units)

Substance	Mass (kDa)	Ellipsoid half-axis (hard core) (nm^3)
Ribosome	4.200	30 × 20 × 20
RNA polymerase II	500	26 × 14 × 14
GFP PCNA trimer	180	11 × 11 × 11
Streptavidin	53	5 × 4 × 4
Chromatin segment	9.750	150 × 30 × 30

Diffusion

First of all the diffusion of streptavidin throughout rosettes of different intra-rosette spacings is estimated (Fig. 1).

Simulations are done for intra-rosette spacings of 2.5, 10.0, 21.1, and 27.3 nm. Figure 2 shows the diffusive behaviour for all of the simulated substances. Qualitatively, the straight lines describe regular diffusion for all substances. This behaviour is observed for all of the simulated intra-rosette spacings, hence the plot for 27.3 nm is exemplary and the ones for the other distances are omitted. Obviously the streptavidin-sized particles diffuse much faster than the ribosome-sized particles, but even the large "ribosome" particles diffuse regularly. A complete overview of all the diffusion constants for all substances and spacings is shown in Table 3, which shows that, for the same substance and different spacings, the diffusion

Table 2 Lennard–Jones force field parameters for the different substances: the potential starts at the hard core (Table 1) and ends after the cutoff

Substance	Potential	Cutoff (nm) r_c
Ribosome	r^{-6}	7
RNA polymerase II	r^{-6}	4
GFP PCNA trimer	r^{-6}	3
Streptavidin	r^{-6}	1
Chromatin segment	r^{-6}	8

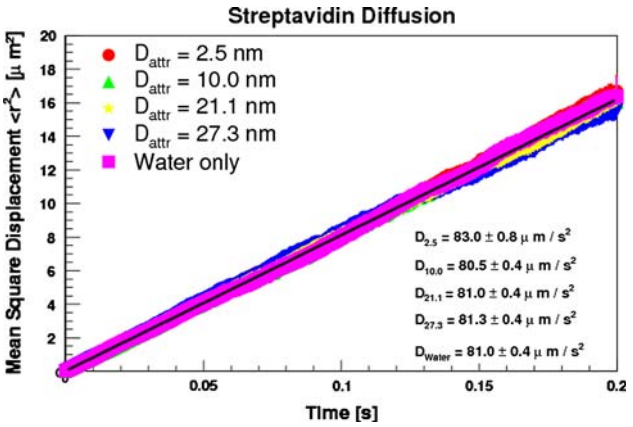

Fig. 1 Mean-square displacements of calculated diffusion patterns of modelled streptavidin complexes for four different intra-rosette spacings

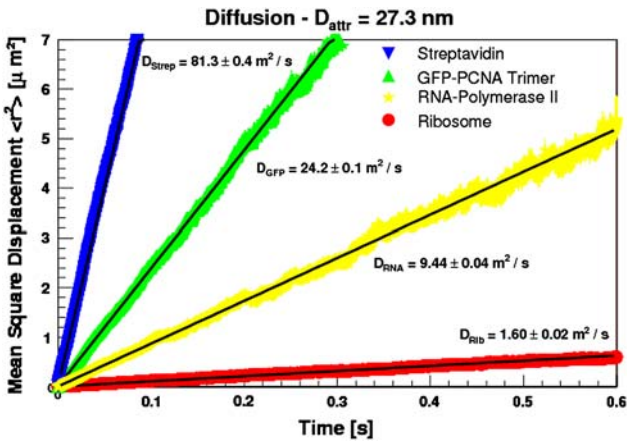

Fig. 2 Mean-square displacements of calculated diffusion patterns for all modelled substances. Regular diffusion was observed independent of the size of the moving complexes. The diffusion constants are stated for a intra-rosette spacing of 27.3 nm

constants do not differ much; within errors they are essentially the same. Error bars for the 2.5 nm spacing are larger because the sample size is smaller.

Accessibility

The accessibility of the rosettes is of major interest. To shed light on this matter we investigate the density of the substance at different z-slices around the core of the rosette. Figure 3 shows these slices for the two extreme intra-rosette spacings of 2.5 nm on the left-hand side and 27.3 nm on the right-hand side. Slices at $z = -100$, 0 and 100 nm from the core are shown. One can observe that the core of the small spacing remains compact while that of the large spacing is more smeared out. The core of the larger spacing is obviously slightly larger, but its boundaries are less well defined than for the smaller spacing.

The relative density of the "streptavidin" particles in the 27.3-nm rosette with respect to the water-only run is shown in Fig. 4. As a particle approaches the centre of the rosette the density rapidly declines. The innermost part is absolutely inaccessible ($\rho = 0$). The density ρ can be described by the following fit function:

$$\frac{\rho}{\rho_{\text{bulk}}} = 1 - e^{-\frac{r-\Delta r}{r_0}}, \quad (1)$$

where r_0 is a measure for the opalescence of the rosette. For small r_0 a penetrating molecule does not notice the rosette until it almost touches the impenetrable hard core region of Δr ($r \geq \Delta r$ for all r values). If r_0 is much larger than 1 the molecule already feels the repulsion from far away.

If one fits the density with Eq. 1 one obtains a fit value of $\Delta r = 20.1 \pm 3$ nm and $r_0 = 69.0 \pm 6$ nm. Therefore the excluded volume in the centre of the rosette is a sphere of about 40 nm diameter. This volume comprises 6 ± 2 kbp of the rosette fiber (total rosette length assumed: $\sim$1Mbp). If one associates r_0 with an average penetration depth, then the DNA between 20 and 69 nm from the core is difficult to access. This corresponds to 79 ± 8 kbp of DNA which is difficult to access, as illustrated in Fig. 5.

It is obviously also interesting to see how ribosome-sized protein complexes can penetrate the rosette. All the values of r_0 and Δr for "streptavidin" and "ribosome" particles are listed in Table 4. There is one trend independent of the substance: for the larger core the particles seem to be able to penetrate into the deep core more easily while the average penetrability is less than for the dense core. This means that a larger core has a greater extension but is less dense and thus particles can occasionally reach further into the core but are in general further away from it. A dense core is basically concentrated at the centre and no particles can penetrate deep inside the core. For the large-sized ribosome particles, obviously an increase of the parameters r_0 and Δr can be shown. Therefore for the $D_{27.3\ \text{nm}}$ rosette approximately 12 ± 3 kbp are totally

Table 3 Estimated diffusion constants D for different intra-rosette spacings

Intra-rosette spacings Substance (size correspondence)	27.3 nm D ($\mu m^2/s$)	21.1 nm D ($\mu m^2/s$)	10.0 nm D ($\mu m^2/s$)	2.5 nm D ($\mu m^2/s$)
Ribosome	1.60 ± 0.02	1.61 ± 0.02	1.64 ± 0.02	1.69 ± 0.05
RNA polymerase II	9.44 ± 0.04	9.46 ± 0.04	9.51 ± 0.05	9.73 ± 0.17
GFP PCNA trimer	24.2 ± 0.1	24.3 ± 0.1	24.4 ± 0.1	24.4 ± 0.3
Streptavidin	81.3 ± 0.4	81.0 ± 0.4	80.5 ± 0.4	83.0 ± 0.8

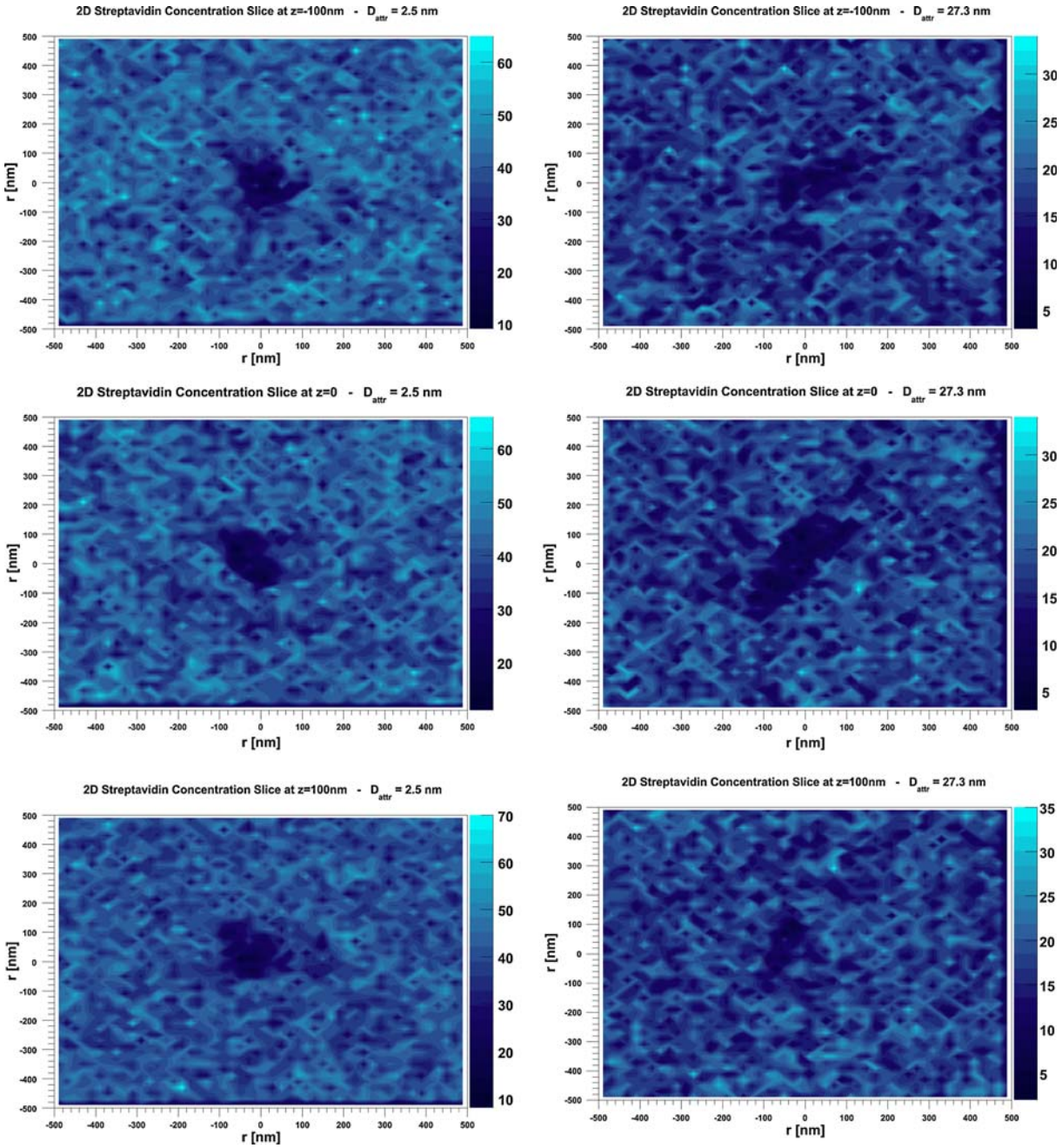

Fig. 3 Two-dimensional density plot of 7,000 configurations. The images on the left show a compact 2.5-nm core while the ones on the right show a 27.3-nm core. For larger intra-rosette spacings the rosette core is smeared out and more penetrable

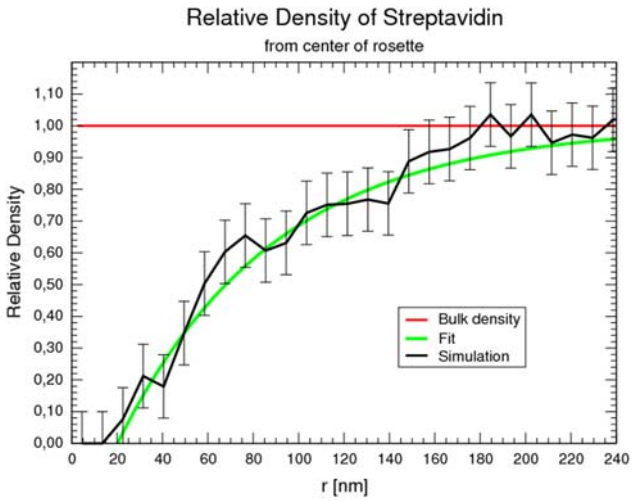

Fig. 4 Relative density from the centre of the $D_{27.3\ \mathrm{nm}}$ rosette. As one approaches the inner core, the density continually decreases. The fit function and values are stated in the text

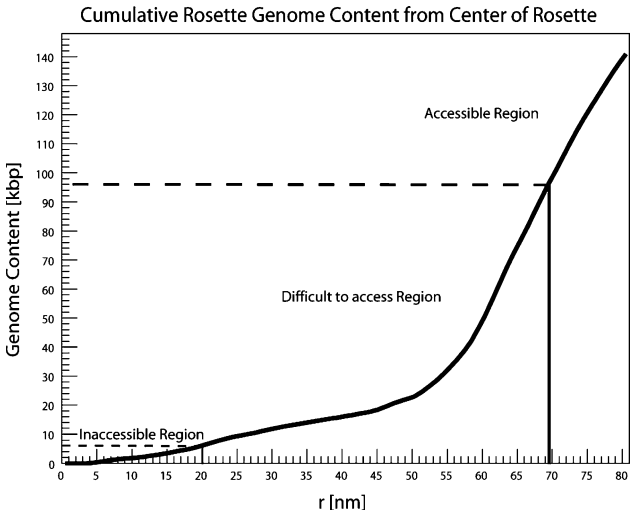

Fig. 5 Cumulative genome content with respect to the centre of the rosette. One can observe three regions of different accessibility

Table 4 Values of Δr and r_0 for streptavidin and ribosome-sized proteins for the $D_{27.3\ \mathrm{nm}}$ and $D_{2.5\ \mathrm{nm}}$ rosettes

Substance	$D_{27.3\ \mathrm{nm}}$		$D_{2.5\ \mathrm{nm}}$	
	Δr (nm)	r_0 (nm)	Δr (nm)	r_0 (nm)
Streptavidin	20.1 ± 3	69.0 ± 6	26.21 ± 3	60.9 ± 5
Ribosome	27 ± 5	143 ± 6	32 ± 5	110 ± 6

inaccessible to Ribosomes, while 190 ± 8 kbp of DNA is difficult to access.

The average density drop-offs (a drop-off of, e.g. 0.3 means that the intensity under a microscope would drop from 1.0 to 0.7) are shown in Table 5. This decrease in intensity is equivalent to an intensity drop-off observed by a line-scan analysis under a microscope. Therefore we predict a decrease in fluorescence intensity of about 30% in heterochromatic clusters.

Table 5 Average density drop-off (a drop-off of e.g. 0.3 means that the intensity under a microscope would drop from 1.0 to 0.7) for the different intra-rosette spacings

Intra-rosette spacing (nm)	Average density drop-off
27.3	0.33 ± 0.05
21.1	0.38 ± 0.05
10.0	0.30 ± 0.05
2.5	0.23 ± 0.04

Conclusions

The simulations have revealed several noteworthy results. First of all, an overall regular diffusion was observed for all substances and for all intra-rosette spacings. If particles diffuse anomalously in the nucleus then it is not due to the physical restriction of the rosettes and their cores, at least not on the scale of a single rosette. Even the relatively large ribosome-sized particles access nearly as much of the rosette as the smaller particles. This is supported experimentally by Politz et al. (2003), although they measured anomalous diffusion on a larger scale. Furthermore, the size of the spacing was basically irrelevant for the diffusion constants.

The second part of the analysis focussed on the accessibility of the rosette. It could be shown that the centre of a rosette is inaccessible for all spacings. From the simulation results one can conclude that intra-rosette spacings from 2.5 to 27.3 nm yield density drop-offs between 23% and 38%. Even though, most of the rosette is accessible even to large molecule complexes such as ribosome-sized particles, a small region in the centre of the rosette is not. A promoter region is 3 kbp in length, which is comparable to the inaccessible genome in the centre of the rosette. Therefore if exactly this promoter region is inaccessible, the RNA polymerase may not bind and the entire gene may not be transcribed. Therefore our results show that the silencing of genes in the 1-Mbp chromatin domains could possibly be caused solely by physical inaccessibility. These predictions are well compatible with the findings of Verschure et al. (2003) based on conventional microscopy observations. As Figs. 3, 4, and 5 indicate, in a conventional microscopic observation volume corresponding to a diameter of ~250 nm (the optical resolution limit in conventional light microscopy), only a region with a diameter of ~40 nm is inaccessible, i.e. about 0.5% of the minimal observation

volume. Such a small region of inaccessibility is far below the detection limits of conventional light microscopy.

These findings might be interpreted in the light of tracking experiments of single streptavidin molecules in structurally and functionally distinct nuclear compartments. The experimental results indicated that all nuclear subcompartments were easily and similarly accessible for such an average-sized protein, and even condensed heterochromatin neither excluded single molecules nor impeded their passage (Grünwald et al. 2008). However these streptavidin molecules did not accumulate in heterochromatin, suggesting comparatively less free volume.

Regarding the limited optical resolution of the far-field light microscopy approach used, the predictions of the nanostructure model presented here might be compatible with the available conventional light microscopy data. To test the predictions of this and other nanostructure models concerning small regions of inaccessibility, light microscopic techniques with an effective resolution in the few nanometer range are required. Appropriate techniques to achieve such a resolution are presently under development. In addition to stimulated emission depletion (STED) microscopy with an optical resolution of about 15 nm (Donnert et al. 2006), methods of spectrally assigned localisation microscopy such as spectral precision distance microscopy (SPDM) (e.g. Esa et al. 2000), or photoactivated localisation microscopy (PALM/FPALM/PALMIRA) (Betzig et al. 2006) might be used. These methods are expected to allow an effective optical resolution down to few nanometres.

Acknowledgments For many helpful discussions and remarks, and for reading and correcting the manuscript we thank Prof. Dr. C. Cremer. For financial support the authors thank the German Science Foundation (DFG) in project DFG KR 2213/2-2.

Simulation techniques

Polymer model

To model the polymer backbone of the chromatin fiber, the continuous backbone mass model was used (Schöppe and Heermann 1999). In contrast to the commonly used bead-spring model, here non-spherical force fields are applied for the non-bonded interaction. By this procedure the possible anisotropy of a group of atoms which has to be course-grained in a construction unit can be taken into account. The simplest anisotropic geometrical object one can think of is an ellipsoid of rotational symmetric form, which is used also for the present simulations. Besides the bonded interaction between adjacent segments, also non-bonded interactions between different segments have to be taken into account. Here we apply the repulsive part (or, respectively, the attractive and the repulsive part) of the Lennard–Jones force field to model the non-bonded interactions between repulsive (respectively, attractive) segments. Debye-type electrostatic interactions are expected to be limited to a range <10 nm (compare Münkel and Langowski 1998) and can therefore be neglected for such large-scale simulations.

In the following a list of parameters and model parameterisations for the simulations is given:

- Segment diameter: 30 nm
- Kuhn length of 15 kbp corresponds to a segment length of 150 nm
- The harmonic bond potential is taken to be

$$U_{\text{bond}}(l) = \frac{k_b T}{2\delta^2}(l - l_0)^2 \tag{2}$$

  with $\delta = 0.1$ and $l_0 = 150$ nm at 310.15 K
- The angular and torsional potentials are taken to be 0. On this scale the chain is flexible.
- Repulsive segment potential:

$$U_{\text{rep}}(r) = \varepsilon\left(\frac{\sigma}{r - r_{\text{segment}}}\right)^6 \tag{3}$$

  with $\varepsilon = 0.14 k_B T$ at body temperature, $\sigma = 15$ nm, and $r_{\text{segment}} = 15$ nm being the fiber radius
- Cutoff for the repulsive potential is $r_c = 8$ nm (after the 15 nm fiber radius).
- Attraction segment potential

$$U_{\text{attr}}(r) = 4\varepsilon\left[\left(\frac{\sigma}{r - r_{\text{segment}}}\right)^{12} - \left(\frac{\sigma}{r - r_{\text{segment}}}\right)^6\right]$$

  with $\varepsilon = 7 k_B T$ at body temperature and σ was taken to be 2.5, 10.0, 21.1 or 27.3 nm.
- Cutoff for the Lennard–Jones potential is $r_c = 80$ nm (after the 30 nm fiber diameter)

The spring constant $\delta = 0.1$ was chosen such that the 150-nm segment was reasonably stiff and at the same time soft enough to ensure a reasonable integration time step. For the Lennard–Jones potential $\varepsilon = 7 k_B T$ was chosen because this proved to be the smallest potential depth for which the segments remain attractive at body temperature. The analogous reasoning applies to $\varepsilon = 0.14 k_B T$ for the repulsive potential.

Relaxation

A starting configuration for the Brownian dynamics simulation run is obtained by molecular dynamics (MD) relaxation as described in Odenheimer et al. (2005). After an initial rise, this is due to the random and hence mostly unphysical starting configuration, the maximum extension of

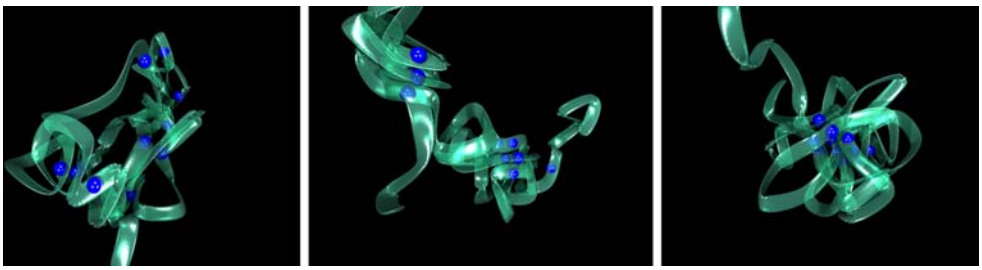

Fig. 6 *Left* a starting configuration of a 60-segment chromatin fiber. The *spheres* represent the attractive sites. *Centre*: an intermediary configuration. This state of mainly two clusters of approximately equal size turns out to be a metastable state. *Right*: in the final state all attractive segments are concentrated in the centre. A rosette has formed

the initial structure decays over a time of about 10,000 MD steps. After this time the distance drops no more, hence all attractive segments have found each other. The fully equilibrated structure is shown to be a rosette (compare Fig. 6).

Brownian dynamics

The 1.2-Mbp chromatin rosette was put in a simulation box of $1 \times 1 \times 1\ \mu m^3$ with periodic boundary conditions. The chromatin rosette had a diameter of about 800 nm. Thus the average distance between rosettes was about 200 nm. A closer packing of rosettes, i.e. a smaller simulation box, was not possible because of the necessity to generate a feasible starting configuration. The starting configuration was generated as follows. First an already condensed rosette (see previous section) was moved to the centre of the simulation box. Then a spherical shell with a radius of 900 nm was tessellated into a 1,024-on. At each vertex of the 1,024-on a particle was placed. This starting configuration was then equilibrated with dissipative particle dynamics (DPD) until a random distribution was achieved. This configuration was then the new starting configuration for one DPD run. For such simulation techniques the mass of the diffusing particles is immaterial; only for an estimation of the integration time step is the mass of the smallest diffusing protein (here streptavidin) regarded. The detailed justification of this method and itssuperiority over regular Brownian dynamics, especially for block copolymers, is described by Frenkel and Smit (2002).

Statistics

One simulation consists of one substance at one intra-rosette spacing. Ten runs were computed for each simulation; each run consists of 7,000 uncorrelated configurations. Simulations were done for all substances at all intra-rosette spacings. For the streptavidin and ribosomes, a run without the rosette structure was performed first to obtain simulation data in water only. The simulation box and duration was the same as for the latter runs with the rosette. The streptavidin water-only run was used to calibrate the time scale.

References

Betzig E, Patterson GH et al (2006) Imaging intracellular fluorescent proteins at nanometer resolution. Science 313:1642–1645

Bohn M, Heermann DW et al (2007) A random loop model for long polymers. Phys Rev E Stat Nonlin Soft Matter Phys 76:051805. doi:10.1103/PhysRevE.76.051805

Bon M, Marenduzzo D et al (2006) Modelling a self-avoiding chromatin loop: relation to the packing problem, action-at-a-distance, and nuclear context. J Cell Sci 14(2):197–204

Cremer T, Cremer C (2001) Chromosome territories, nuclear architecture and gene regulation in mammalian cells. Nat Rev Genet 2(4):292–301. doi:10.1038/35066075

Donnert G, Keller J et al (2006) Macromolecular-scale resolution in biological fluorescence microscopy. Proc Natl Acad Sci USA 103:11440–11445. doi:10.1073/pnas.0604965103

Esa A, Edelmann P et al (2000) Three-dimensional spectral precision distance microscopy of chromatin nanostructures after triple-colour DNA labelling: a study of the BCR region on chromosome 22 and the Philadelphia chromosome. J Microsc 199(2):96–105. doi:10.1046/j.1365-2818.2000.00707.x

Frenkel D, Smit B (2002) Understanding molecular simulation from algorithms to applications. Computational science from theory to applications, vol 1, 2nd edn. Academic Press, San diego

Gorisch SM, Wachsmuth M et al (2005) Histone acetylation increases chromatin accessibility. J Cell Sci 118(24):5825–5834. doi:10.1242/jcs.02689

Grünwald D, Martin RM et al (2008) Probing intranuclear environments at the single-molecule level. Biophys J 94:2847–2858. doi:10.1529/biophysj.107.115014

Marenduzzo D, Faro-Trindade I et al (2007) What are the molecular ties that maintain genomic loops? Trends Genet 23(3):126–133. doi:10.1016/j.tig.2007.01.007

Münkel C, Langowski J (1998) Chromosome structure predicted by a polymer model. Phys Rev E Stat Phys Plasmas Fluids Relat Interdiscip Topics 57:5888–5896. doi:10.1103/PhysRevE.57.5888

Nicodemi M, Prisco A (2009) Thermodynamic pathways to genome spatial organization in the cell nucleus. Biophys J 96:2168–2177. doi:10.1016/j.bpj.2008.12.3919

Odenheimer J, Kreth G et al (2005) Dynamic simulation of active/inactive chromatin domains. J Biol Phys 31(3):351–163. doi:10.1007/s10867-005-7286-3

Ostashevsky J (1998) A polymer model for the structural organization of chromatin loops and minibands in interphase chromosomes. Mol Biol Cell 9(11):3031–3040

Politz JC, Tuft RA et al (2003) Diffusion-based transport of nascent ribosomes in the nucleus. Mol Biol Cell 14(12):4805–4812. doi:10.1091/mbc.E03-06-0395

Roh TY, Cuddapah S et al (2005) Active chromatin domains are defined by acetylation islands revealed by genome-wide mapping. Genes Dev 19(5):542–552. doi:10.1101/gad.1272505

Schöppe G, Heermann DW (1999) Alternative off-lattice model with continuous backbone mass for polymers. Phys Rev E Stat Phys Plasmas Fluids Relat Interdiscip Topics 59:636–641. doi:10.1103/PhysRevE.59.636

Strahl BD, Allis CD (2000) The language of covalent histone modifications. Nature 403(6765):41–45. doi:10.1038/47412

Verschure PJ, van der Kraan I et al (2003) Condensed chromatin domains in the mammalian nucleus are accessible to large macromolecules. EMBO Rep 4(9):861–866. doi:10.1038/sj.embor.embor922